Cytometry 9:418–425 (1988)

Interval-Coded Texture Features for Artifact Rejection in Automated Cervical Cytology

James H. Tucker, Karsten Rodenacker, Uta Juetting, Peter Nickolls, Keith Watts, and Georg Burger

Clinical and Population Cytogenetics Units, Medical Research Council, Edinburgh EH4 2XU Scotland (J.H.T.); Mathematical Physics Group, Institut für Strahlenschutz, Gesellschaft für Strahlen und Umweltforschung, D-8042 Neuherberg, Federal Republic of Germany (K.R., U.J., G.B.); Department of Electrical Engineering, Sydney University, Sydney, Australia (P.N.); Department of Cytopathology, Charing Cross Hospital, London W68RF, England (K.W.)

Received for publication September 23, 1987; accepted April 4, 1988

In order to improve the separation between abnormal cells and noncellular artifacts in the CERVIFIP automated cervical cytology prescreening system, 22 different object texture features were investigated. The features were all statistical parameters of the pixel density histograms or one-dimensional filtered values of central and border regions of the object images. The features were calculated for 231 images (100 cells and 131 artifacts) detected as Suspect Cells by the current CERVIFIP and were then tested in hierarchical and linear discriminant classifiers. After selecting the two best features for use in a hierarchical classifier, 83% correct classification was achieved. One of these features was specifically designed to remove poorly focused objects. With maximum likelihood discrimination using all 22 features, an overall correct classification rate of 90% was obtained.

Key terms: Image analysis, pattern recognition features, automated prescreening, cervical cytology chromatin, texture, artifacts

The problem of rejecting noncellular artifacts is one of very great practical importance in automated cytometry. For example, a major difficulty in cervical cytology automation is that of rejecting false-alarm signals ("false positives") in normal specimens caused by artifacts such as overlapping cell pairs, leukocyte clusters, dust particles, etc. Already, several techniques have been developed for this purpose based upon the analysis of global object features (e.g. area, density) (14,19), object shape (6,14,16–18,24,25), object texture (6), and object colour (6). Nevertheless, it has been found in system trials that a significant number of artifacts are not detected using classification based upon these features, so that false-positive objects are still a major factor in specimen misclassification. Improvements in features for artifact rejection should therefore result in an increased efficiency of such systems.

The analysis of cellular texture is one of the major areas of research in the extraction of information from cell images. Several different approaches have emerged, including the use of co-occurence (transition) matices (23), grain analysis (13), one- and two-dimensional filtering (10), run-length texture analysis (8), and statistical parameters (1). In quantitative cytology, the analysis of nuclear texture has been particularly successful in separating normal and malignant specimens, even in apparently normal cells, (3,4), because texture measurements on an appropriately prepared and stained cell nucleus reflect the local chromatin arrangement, which is one of the most powerful indicators of cell function and hence of cell pathology.

One type of instrumentation that has found application in the field of automated cytometry is that of the continuous motion imaging (CMI) system, in which the specimen is moved continuously under a one-dimensional scanner (e.g., linear CCD diode array) (2,12,15). These systems possess several desirable properties for cervical cytology automation; they are fast, and they have potentially good resolution and signal/noise characteristics (21). However, such systems present special constraints on the data analysis process. The data analysis must be sufficiently fast to take advantage of the high scanning rates possible in the scanner; this probably requires a mixed hardware/software solution. Also, in spite of the good potential resolution of the scanner, the overall system resolution may be locally reduced because of the practical difficulty of maintaining accu-

Address reprint requests to James H. Tucker, Ph.D., M.R.C. Clinical and Population Cytogenetics Unit, Western General Hospital, Crewe Rd., Edinburgh, EH4 2XU, UK.

This work was supported by the U.K. Medical Research Council and the Gesellschaft für Strahlen und Umweltforschung, FRG.

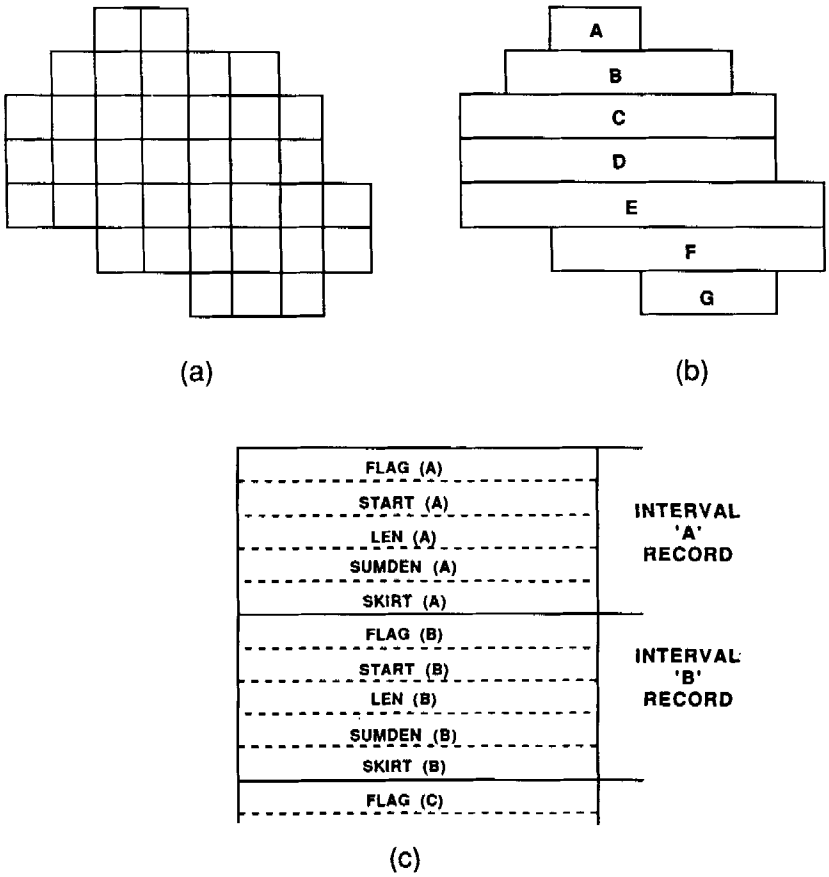

FIG. 1. Interval coding data compression. **a:** Original pixels forming an object. **b:** Interval representation; each interval incorporates the object's pixels in one scan line. **c:** Interval data words loaded into the computer. Flag words contain articulation data; start, length (LEN), and sumden words summarise the values from the interval's pixels, and skirt words contain the local background density data.

rate image focus as the specimen is traversed. Thus, the techniques must be suitable for hardware/software implementation and must operate in medium-resolution conditions.

This paper describes a preliminary study to investigate the artifact/cell discrimination properties of one class of object texture features that are particularly suitable for implementation in CMI scanners. Of the various classes of texture features mentioned above, those based on one-dimensional filters are particularly suitable for this type of scanner. The techniques are relatively simple and may be implemented in hardware, and it is unlikely that the obvious difficulty of directionality would pose serious problems in their application to randomly oriented cell and object images. The detailed aim of this investigation was therefore to select, using off-line image analysis of object images classified as suspicious cells by the existing cell classifier, a small number of texture features based on one-dimensional statistical properties for full hardware/software implementation in the real-time CERVIFIP scanning system.

MATERIALS AND METHODS

The CERVIFIP System

The CERVIFIP automated cervical cytology prescreener has been described fully elsewhere (20), but for completeness it will be outlined here. The system is based on the "fast interval processor," a continuous motion imaging (CMI) analysis system in which high scanning and object classification rates are obtained using a linear diode array scanner and combined hardware/software analysis. The system detects neoplastic specimens by locating cells with an abnormally high DNA content so that they can be inspected and diagnosed by a cytotechnologist. It does this by a high-speed scan during which a two-stage classifier notes and records the positions of suspicious objects. These can later be relocated for visual diagnosis by a cytotechnologist.

Texture Features Investigated

The texture features investigated in this study were selected initially as being potentially suitable for imple-

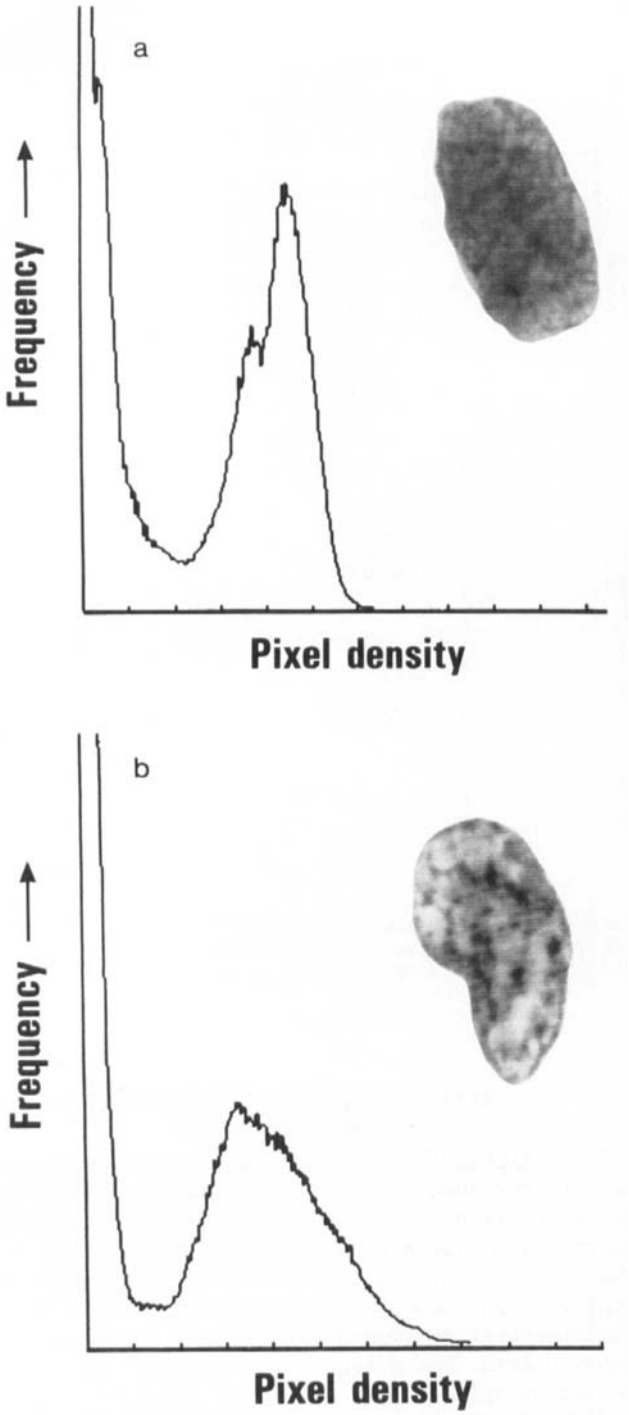

FIG. 2. Images and density histograms from images of cell nuclei. Histogram a, with little chromatin; b, with prominent, clumped chromatin. The low-density peaks arise from pixels in the background region.

mentation in the "interval coding" data compression technique used in the fast interval processor (Fig. 1). One type of texture feature that fulfills this requirement is that of statistical parameters from direct or one-dimensional filtered images (1,10). Typical density histograms for two cells with different degrees of chromatin clumping are shown in Figure 2. Various statistical features can be calculated for these histograms such as:

number:

$$DEN0 = \sum_{i=0}^{i=I} n(i)$$

mean:

$$DEN1 = \frac{\sum_{i=0}^{i=I} \sum_{p=0}^{p=n(i)} D(i,p)}{DEN0}$$

standard deviation:

$$DEN2 = \frac{\sum_{i=0}^{i=I} \sum_{p=0}^{p=n(i)} (D(i,p))^2}{DEN0} - DEN1^2$$

where $D(i,p)$ = density of pixel p in interval i, $n(i)$ = number of pixels in interval i, I = number of intervals in object.

In an interval coding system, these features can be computed with interval coding hardware, which generates values for

$$n(i)$$

$$\sum_{p=0}^{p=n(i)} D(p)$$

$$\sum_{p=0}^{p=n(i)} (D(p))^2$$

in each interval.

A second group of histograms and features can be generated with data produced from one-dimensional filters such as a difference filter, where each histogram entry D at pixel p is replaced in the three equations above by

$$E(p) = D(p) - D(p-1)$$

Another potentially useful feature that can be easily obtained in interval-coding hardware is the "deviance" of each interval, defined as

$$V(i) = Dm - \frac{\sum_{p=0}^{p=n(i)} D(p)}{n(i)}$$

where Dm = maximum $D(p)$ occurring within the interval. The mean and standard deviation can then be obintervals in the object.

One of the major problems of texture measurements is that they are strongly affected by object boundaries. The overall texture measurement from an object will be made up from contributions from density changes at bounda-

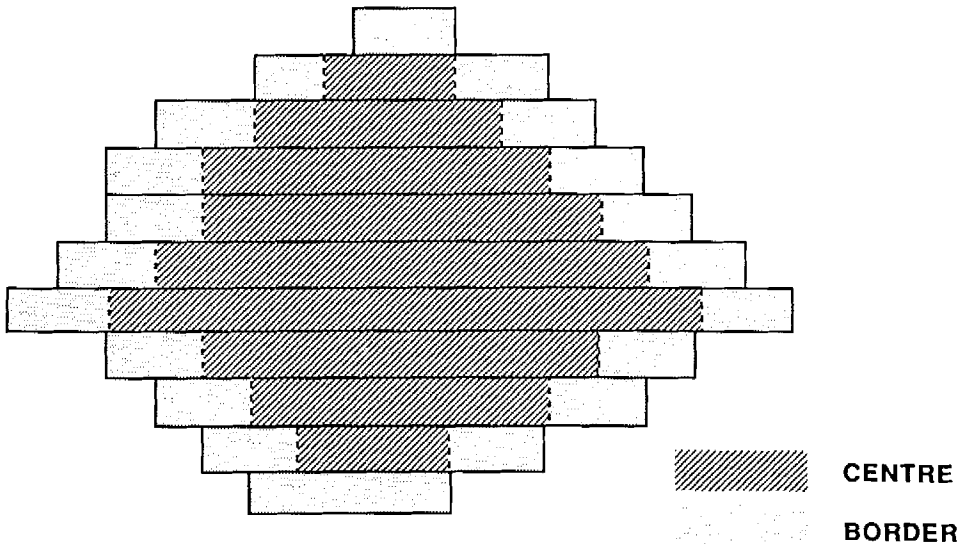

FIG. 3. Centre and border regions of cell nucleus image. The first and last b pixels (where b is the border width) are taken as border-region pixels; the remainder are centre-region pixels.

Table 1
CERVIFIP Classifier Limits for Search Scans
(See ref. 21 for details of tests)

Primary classifier limit (all objects):	
IOD > 2.2 × histogram mode	
Secondary classifier Limits (high-IOD objects only):	
Mean density	<91
Chord test	<17
Box test	<15
Perimeter tests	<4
Ellipse test	<23

ries, and from centre-region differences caused by true textural properties. These can be separated by calculating separate histogram features for image data from the "centre" region (CDEN0, CDEN1, CDEN2) and from the "border" region (BDEN0, BDEN1, BDEN2) of each interval generated from an object image (Fig. 3).

Another potential problem that may be helped by this distinction is that of object focus. In central regions of an object, the measured values will be affected by both object focus and the object textural properties. However, in the region of the sharp nuclear boundary, texture measurements will be predominantly affected by the resolution properties of the analysis system (modulation transfer function, focus, etc.). Thus boundary-region texture measurements may be expected to reflect object focus.

In these experiments, a border region size of 2 pixels was used. This was selected to suit the resolution characteristics of the CERVIFIP system on which the images were scanned by eliminating most of the transient response region from sharply focused edges (previously measured as 2.5–4 pixels) (21), while leaving the maximum centre-region area for textural analysis.

Image Data Base Collection

The object images used for the experimental investigations were obtained from 20 cervical cytology scrape specimens with varying cytological grades. Slides were prepared using the suspension/monolayering/gallocyanin chrome alum method developed for use with the CERVIFIP system (11,22). The CERVIFIP system program was then set up to determine the positions of high-DNA objects detected as suspect cells, using a previously optimised classifier for abnormal cell detection and artifact rejection. The artifact rejection features used in this classifier are as used in a previous system (19), with the limits set on each feature as given in Table 1. For each slide, a 0.5 × 0.5-cm area was scanned, and the detected objects were relocated and visually classified as nuclei (true positives) or artifacts (false positives) by one of us (K.W.). The total number of cells scanned and the number of detected objects (abnormal cells and artifacts) in each specimen are shown in Table 2.

In order to obtain the pixel density data for further analysis, the detected objects on each specimen were then individually relocated, focused visually, and rescanned using the CERVIFIP "frame scan" facility. In all cases, the digitisations were 64 × 64 pixels, at a typical scanning resolution of the CERVIFIP system (i.e., pixel size 0.5 × 0.65 μm, with a gray-level resolution of 256 × 0.005 optical density units). A total of 273 images (114 abnormal nuclei and 159 artifacts) were digitised; Figure 4 shows a selection of typical object images from the data base.

Image Processing

All image data were transferred to the BASISS (BildAnalyse System Institut fur StrahlenSchutz), a high-resolution cell image analysis system set up on a

Table 2
Data Base Selection—CERVIFIP Scan Results

Specimen	Diagnosis	Total cells	Detected objects	Visual class	
				Abnormals	Artifacts
S793	CIN2	27,187	24	15	9
S799	CIN3	17,955	18	10	8
S696	CIN2	3,006	9	7	2
S840	CIN3	14,579	10	9	1
S815	CIN2	23,683	16	15	1
S800	CIN2	20,077	29	10	19
B1310	IIR	6,735	37	8	29
B6143	N	2,290	15	4	11
B1324	II	1,211	8	2	6
S851	IIR	8,410	2	1	1
S728	CIN3	1,586	4	1	3
S695	CIN1	2,622	2	2	0
B1364	IIR	12,537	32	3	29
B1290	N	4,426	16	0	16
S727	CIN3	8,729	10	4	6
S953	CIN3	11,856	10	6	4
S931	CIN1	6,645	5	5	0
S805	CIN2	10,905	10	8	2
S872	INV	3,503	4	3	1
S670	CIN3	12,870	12	1	11
Total		200,822	273	114	159

Table 3
Object Global and Texture Features Evaluated

Name	Description
Global features	
TAREA	Total area
TIOD	Total integrated optical density
CDEN1	Mean of density histogram of centre region
BDEN1	Mean of density histogram of border region
Texture features	
CDEN2	S.D. of density histogram of centre region
CDIF1	Mean of difference histogram of centre region
CDIFI2	S.D. of difference histogram of centre region
BDEN2	S.D. of density histogram of border region
BDIF1	Mean of difference histogram of border region
BDIF2	S.D. of difference histogram of border region
CDEV1	Mean of deviance histogram of centre region
CDEV2	S.D. of deviance histogram of border region
CDEN2C	CDEN2/CDEN1
CDIF1C	CDIF1/CDEN1
CDIF2C	CDIF2/CDEN1
BDEN1C	BDEN1/CDEN1
BDEN2C	BDEN2/CDEN1
BDIF1C	BDIF1/CDEN1
BDIF2C	BDIF2/CDEN1
BDEN2B	BDEN2/BDEN1
BDIF1B	BDIF1/BDEN1
BDIF2B	BDIF2/BDEN1

VAX-750 computer, using the ILIAD (7) interactive picture processing language. In BASISS, the images were segmented using a fixed-level threshold corresponding to that used in the CERVIFIP system and cleaned to remove extraneous above-threshold areas. Subsequently, a code representing the focus accuracy of the rescanned object image (1–4, where 1 = poor focus, 4 = excellent focus) was added after visual inspection of the image.

The images were processed with ILIAD/BASISS external procedures (written in "C"), which generated interval records for each image and then computed a group of four global features and 18 density, difference, and deviance texture features for each object. A full list of the calculated features is shown in Table 3. In addition to the calculation, ILIAD graphical procedures were used to visualize histograms and individual interval values accumulated during the computation of each feature.

The features were input to the BMDP classification program (5) for the generation of feature histograms, F-test results, and the design of linear discriminants. Features were also input to the ISPAHAN package (9) for

Table 4
Features Ranked for Best Separation between Good (Group 4) and Poor (Group 1) Focus Objects
(Totals: group 1 = 21; group 4 = 80)

Rank	Name	Limit	Group 1: objects > limit		Group 4: objects < limit	
			No.	%	No.	%
1	BDEN2C	0.078	9	42	1	1
2	BDIF2C	0.055	12	57	1	1
3	BDIF2	3.5	10	47	1	1
4	BDIF1C	0.098	10	47	2	3
5	BDEN2	6.0	8	38	5	6

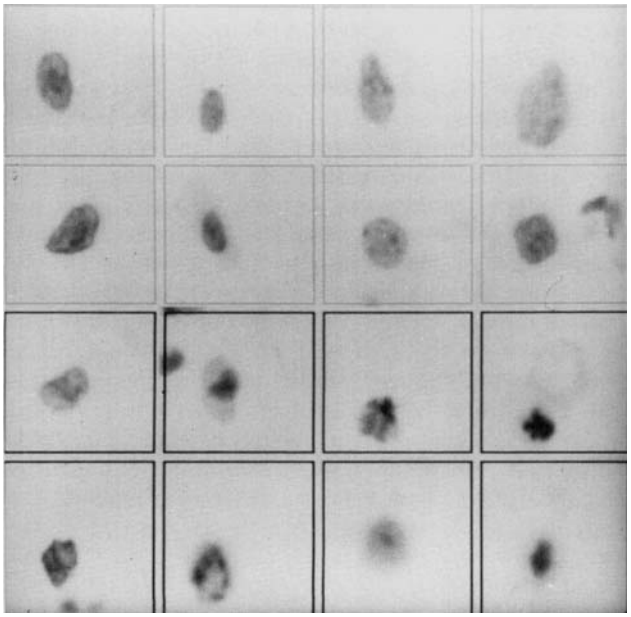

FIG. 4. Typical object images from data base. Light-bordered objects are ATYPical cell nuclei (true positives), and dark-bordered objects are ARTifacts (false positives).

interactive analysis, feature evaluation, and for the design of hierarchical classifiers.

RESULTS

After initial inspection of the 273 images, 42 images were removed from the data base because either the object outline intersected with the border of the scan frame (17 objects), because the feature selection's automatic object selection caused the wrong object to be measured (18 objects), because of lack of certainty of object diagnosis (5 objects), or because the threshold could not be adjusted correctly to give a reasonable separation of the object image from its surrounding background (2 objects).

The remaining 231 objects (nuclei and artifacts) were analysed to find the optimal single-feature discrimination by applying the F-value test to the object population. This test selected CDEV2 as the feature giving the best discrimination between the two classes, but it was clear that this result was much affected by a small group of outliers in the feature distributions, caused by debris particles. When these were removed the cleaned distributions showed CDEN2C to be the best feature, giving an overall accuracy (for all 231 objects) of 82%.

Examination of the object images for misclassified artifacts showed that some of these were poorly focused during the object rescanning process, because of inaccurate setting of the focus by the operator prior to frame scans. Feature selection for the elimination of poorly focused objects was carried out by comparing, for each feature, the error rate for group 4 objects (good focus) for a limit giving an approximately fixed error rate for group 1 (poor focus) objects. Table 4 shows a ranked list of the five best features, together with the discrimination obtained. Histograms for the best feature (BDEN2C with a border width of 2) for both nuclei and artifacts showed a general shift in the modal value as the focus improved.

To investigate the improvement in discrimination possible by using two features rather than a single-feature classifier, a linear discriminant was designed with the two selected features. This gave an overall discrimination of 82%. For comparison, a hierarchical structure was set up with the best selected texture feature (CDEN2C) after removal of objects with a low BDEN2C (<0.1) limit. This strategy gave an insignificant increase in overall discrimination accuracy rate to 83%.

The ISPAHAN maximum likelihood classifier with the overall feature population gave a result of 90% correct classification, obtained from 91/100 (91%) correct nuclei and 116/131 (89%) correct artifacts. Table 5 gives a summary of the best discrimination results obtained with one feature, two features, and all 22 features.

DISCUSSION

The results clearly suggest that image texture features of the type investigated can give useful artifact rejection in CMI and other medium-resolution automated cytometry systems, and in particular can be effective in improving the separation of artifacts and abnormal cell nuclei in CERVIFIP. Although the absolute levels of discrimination obtained in these experiments are of limited interest because of the extreme

Table 5
Classifier Results With One, Two, and 22 (All) Features

	Feature CDEN2C			Features CDEN2C,BDEN2C			22 Features		
	ATYP	ART	% Corr	ATYP	ART	% Corr	ATYP	ART	% Corr
Nuclei	87	13	87	85	15	85	91	9	91
Artifact	28	103	79	25	106	81	15	116	89
Overall			82			83			90

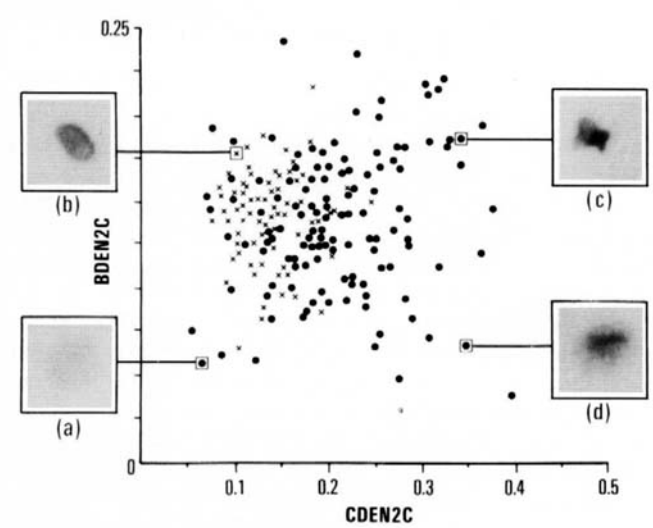

FIG. 5. Typical objects from the BDEN2C-CDEN2C feature space (x = ATYPical cell nuclei ● = ARTifact). Low values of BDEN2C generally indicate poor object focus (**a,d**); for well-focussed objects, CDEN2C separates ATYPical cell nuclei (**b**) and ARTifacts (**c**).

data dependency of the results, comparisons are meaningful because all experiments were carried out on the same data set. With a two-feature hierarchical classifier applied to the 231-object test data base, 81% of the nonnuclear artifacts were eliminated, with a total loss of only 15% of the abnormal nuclei.

The quantitative comparison of results for artifact rejection with other studies is difficult because of the data dependency of the results. Most artifact rejection in the field of cervical cytology automation has been carried out on the basis of shape tests. While these techniques give useful discrimination, they cannot distinguish correctly between single cells and some types of artifact (e.g,. leukocyte on top of squamous cell nucleus). Conversely, such artifacts may be easily distinguished by texture features. Thus, the two domains may be considered to be orthogonal, and complementary in the overall task of artifact/cell discrimination.

In the results obtained in this study, much of the discrimination was obtained from a single feature, CDEN2C. This feature is essentially a contrast-normalised measurement of the width of the peak in the density histogram for the object, and as such gives a good measure of the overall centre-region texture. However, some artifacts gave low CDEN2C values, and the images of these objects showed that some were poorly focused. This fact led to the experiment to evaluate features in terms of focus accuracy, and this clearly demonstrated that the border-zone feature BDEN2C gave the best separation of poor-focus images. Although the improvement in the experimental results obtained with the introduction of this second feature was insignificant, this is because the data base used for these tests contained relatively few poorly focused objects. However, in a practical CERVIFIP implementation its incorporation is likely to be advantageous, because poorly focused images are likely to occur more frequently. In real-time scans, images of objects may be poorly focused for several reasons: the autofocus system may give temporarily incorrect values, because of sparse object population, a dust particle on the slide surface, etc. Also, individual objects may be "floating" in the mounting medium, and so at a different focal plane from other objects in the current field. Such objects frequently cause false-positive signals, since the segmented image and feature values will give a poor representation of the object. The elimination of poorly focused objects could give a particularly useful improvement in CERVIFIP performance.

Examination of the images, basic histograms, interval values, and feature populations revealed several interesting facts. With all of the texture features tested most artifacts (particularly leukocyte clusters and debris particles) gave higher values than the atypical cell nuclei. Overlapping pairs of normal nuclei also gave higher values because of the area of relatively high density of the overlapped region. This is consistent with a previous report concerning transition-matrix measurements from artifacts in Papanicolau-stained smears (6). Thus, most of the artifacts contain areas of widely different density values in comparison to cell nuclei, even those with very pronounced chromatin clumping. The interval value histograms from the deviance parameters show wide variations from interval to interval within the object; this reflects the lack of smoothing in features derived from single-point values. Conversely, interval values from density histogram properties are mostly well smoothed. Another noticeable feature of the results was that most texture feature populations were highly correlated with the mean object density; their classification ability was generally improved (83% correct classifications compared with 80%) by normalisation with the mean density of the centre region.

As with all simulation experiments, caution is needed in interpreting these results, since several important

differences exist between the experimental conditions and the real-worid environment of automated cytometry systems such as CERVIFlP. A typical source of potential inaccuracy arises from the image acquisition method: the data base images were obtained by rescanning the high-IOD objects located during the real-time CERVIFIP scan, so that the object image data may have been different from those analysed during the CERVIFIP scan because of different focus conditions, random noise fluctuations, etc. Again, the classification results obtained are the result of sequential application of the existing shape tests (which were applied in the original CERVIFIP scan) and the texture parameters under evaluation; in real-time application, the sequence and method of application may be further optimised. Last, the results represent the discrimination obtainable on a single data base (without separate learning and test sets); they give no indication of the statistical validity of the values obtained. However, the data base represents the objects selected by the existing CERVIFIP system after scanning a substantial body of typical material (200,822 cells from 20 specimens) and should thus be reasonably representative of real-time scanning conditions and should give a general indication of the power of the features. Further evidence for this is obtained from an inspection of the original images from various regions in the feature-space (Fig. 5), which shows that the features are providing a measure of real physical differences between the two object populations in the data base. Also, the interfeature comparisons should give valid results, since all feature populations were measured under the same conditions.

CONCLUSIONS

The results demonstrate that texture features based on object density histograms can give a useful performance in separating artifacts and single abnormal cell nuclei in automated cervical cytology prescreening systems. Good discrimination was obtained by combining the standard deviation of centre-region density values (to extract object texture) with border-region standard deviation (to detect poor-focus objects). In all cases the discriminant power of the features was improved by normalisation against mean centre-region density.

ACKNOWLEDGMENTS

The authors would like to express their grateful thanks to Dr. N. Louden, Family Planning Association, Edinburgh, and Dr. E. Blanche Butler, Elizabeth Garrett Anderson Hospital, London, for providing specimens for this work. Thanks are also due to Mrs. M. Stark, Medical Research Council Clinical and Population Cytogenetics Unit, Edinburgh, for programming assistance, and to Dipl. Mathr. P. Gais, GSF M.R.G., for his help in transferring the data base. We would also like to thank Dr. D. Rutovitz (Medical Research Council Clinical and Population Cytogenetics Unit, Edinburgh), Dr. O.A.N. Husain (Diagnostic Cytology Laboratory, Charing Cross Hospital, London), and Prof. B. Chaudhuri (Indian Statistical Institute, Calcutta, India) for many helpful discussions and suggestions.

LITERATURE CITED

1. Abmayr W, Giaretti WA, Gais P, Dormer P: Discrimination of G1, S and G2 cells using high resolution TV scanning and multivariate analysis methods. Cytometry 2:316–326, 1982.
2. Bengtsson E. Private communication.
3. Bibbo M, Bartels PH, Sychra JJ, Wied GL: Chromatin appearance in intermediate cells from patients with uterine cancer. Acta Cytol (Baltimore) 25:23–28, 1981.
4. Burger G, Jutting U, Rodenacker K: Changes in benign cell populations in cases of cervical cancer and its precursors. Anal Quant Cytol Histol 3:261–271, 1981.
5. Dixon, WJ. BMDP Statistical Software 1981. University of Califomia Press, Berkeley, 1981.
6. Dytch HE, Bartels PH, Bibbo M, Pishotta FT, Wied GL: The rejection of noncellular artifacts in papanicolau-stained slide specimens by an automated high-resolution system. Anal Quant Cytol Histol 5:241–249, 1983.
7. Eriksson O, Bengtsson E, Jarkrans T, Nordin B, Stenkvist B: Tuning of an interactive software system for image analysis to quantitative microscopy. Proc. International Symposium on Medical Imaging and Image Interpretation (ISMII 82). Berlin, FR Germany 1982. Pub. by IEEE Computer Society, 1982, pp 542–553.
8. Galloway MM: Texture analysis using run lengths. Comput. Graphics Image Process 4:172–179, 1975.
9. Gelsema ES: ISPAHAN Users Manual. Amsterdam Free University, Netherlands, 1985.
10. Giaretti WA, Gais P, Jutting U, Rodenacker K, Dormer P: Correlation between chromatin morphology as derived by digital image analysis and autoradiographic labelling pattern. Anal Quant Cytol Histol 5:79–89, 1983.
11. Husain OAN, Watts KC: The rapid demonstration of nucleic acids using oxidised gallocyanin and chromic potassium sulphate: Methods and applications. J Clin Pathol 37:97–101, 1984.
12. Jaggi P, Poon SSS, Palcic B: Implementation and evaluation of the DMIPS cell analyser. IEEE Proc Eng Med Biol 3:906–911, 1986.
13. Komitowski D, Zinser G: Quantitative description of chromatin structure during neoplasia by the method of image processing: Anal Quant Cytol Histol 7:178–182, 1985.
14. Meyer F: Iterative transformations for an automated screening of cervical smears. J Histochem Cytochem 27:128–135, 1979
15. Shippey G, Bayley RJH, Farrow ASJ, Rutovitz DR, Tucker JH: A fast interval processor. Patt Recog 14:345-365, 1981.
16. Smeulders A: Pattern analysis of cervical specimens. Doctoral Thesis, Leiden University, Leiden, Netherlands, 1983, pp 89–108.
17. Tanaka N, Ikeda H, Ueno T, Watanabe S, Imasato Y: Fundamental study of automated screening for uterine cancer III. New system of automated apparatus (CYBEST) utilizing the pattern recognition method. Acta Cytol (Baltimore) 21:85–89, 1977.
18. Tucker JH, Eason P, Stark MH: Ellipse tests for the reduction of false positive signals in automated cytology. Act Cytol (Baltimore) 22:370–376, 1978.
19. Tucker JH: An image analysis system for cervical cytology automation using nuclear DNA content. J Histochem Cytochem 27:613–620, 1979.
20. Tucker JH, Shippey G: Basic performance tests on the CERVIFIP linear array prescreener. Anal Quant Cytol Histol 5:129–137, 1983.
21. Tucker JH, Husain OAN, Watts K, Farrow S, Bayley R, Stark MH: Automated densitometry of cell populations in a continuous-motion imaging cell scanner. Appl Optics 26:3315–3324, 1987.
22. Watts KC, Husain OAN, Tucker JH, Stark M, Eason P, Shippey G, Rutovitz D, Frost GTB: The use of cationic polyelectrolytes in the preparation of cell monolayers for automated cell scanning and diagnostic cytopathology. Anal Quant Cytol Histol 6:272–278, 1984.
23. Wied GL, Bartels PH, Bibbo M, Sychra JJ: Cytophotometric markers for uterine cancer in intermediate cells. Anal Quant Cytol Histol 2:257–263, 1980.
24. Wheeless LL, Cambier JL, Cambier MA, Kay DB, Wightman LL, Patten SF: False alarms in a slit-scan flow system: Occurrence rates implications and potential solutions. J Histochem Cytochem 27:596–599, 1979.
25. Zahniser DJ, Oud PS, Raaijmakers MCT, Vooys GP, van de Walle RT: BioPepr: A system for the automatic prescreening of cervical smears. J Histochem Cytochem 27:635–641, 1979.